Journal of Applied Fluid Mechanics, Vol. 11, No. 3, pp. 577-584, 2018.
Available online at www.jafmonline.net, ISSN 1735-3572, EISSN 1735-3645.
DOI: 10.29252/jafm.11.03.27230

Numerical Simulation of Turbulent Airflow and Micro-Particle Deposition in Upper Human Respiratory System

A. R. Tahavvor [1†] and P. Zarrinchang [2]

[1] *Department of Mechanical Engineering, Shiraz Branch, Islamic Azad University, Shiraz, Iran*
[2] *Mechanical Engineering Group, Pardis College, Isfahan University of Technology, Isfahan 84156-83111, Iran*

†*Corresponding Author Email: tahavvor@iaushiraz.ac.ir*

(Received September 21, 2016; accepted December 18, 2017)

ABSTRACT

The nasal cavity and sinuses are a component of the upper respiratory system and study the air passage into the upper component of human airway is consequential to amend or remedy deficiency in human respiration cycle. The nose performs many paramount physiological functions, including heating, humidifying and filtering inspired air, as well as sampling air to smell. Aforetime, numerical modeling of turbulent flow in authentic model of nasal cavity, sinus, pharynx and larynx has infrequently been employed. This research has tried to study details of turbulent airflow and particle deposition through all spaces in three-dimensional authentic model of human head which is obtained from computed tomography scan images of a 26-years old female head, neck and chest without any problem in her respiratory system that air can flow them. The particle size in this study was opted to be in the range of 5-30 μm. The particles are tracked through the continuum fluid discretely utilizing the Lagrangian approach.

Keywords: Nasal cavity; Micro-particle; Turbulent flow; CFD; Respiratory system.

NOMENCLATURE

A	cross-sectional area	Re	Reynolds number
B	buoyancy force	t	time
D	drag force	T	turbulent
D	diameter	u	speed
h	hydraulic	y	viscous sublayer
in	inlet	v	viscosity
I	turbulent intensity	VM	virtual mass force
K	turbulent kinetic energy		
m	mass	ρ	density
P	pressure gradient force	τ	reynolds stress tensor
p	pressure	ω	specific rate of dissipation

1. INTRODUCTION

The sinuses and nasal cavity are a component of the system of human respiration. This system carries out some physiological activities, including humidifying, filtering and heating inlet air, like smelling. Also, the nose filters inlet air from pollutant and toxic particle to enter the airway. Major development in the particle transfer, drug distribution and toxicology to filtration of particles from the atmosphere during respiration and surgeries could be observed through an amended understanding of the fluid flow details thru the human upper airways. So study the air flow in the human respiratory system such as nose, nasal cavity and sinuses is paramount to amend defects in breathing cycle. Aerosol transport and deposition in respiratory system has been studied numerically and

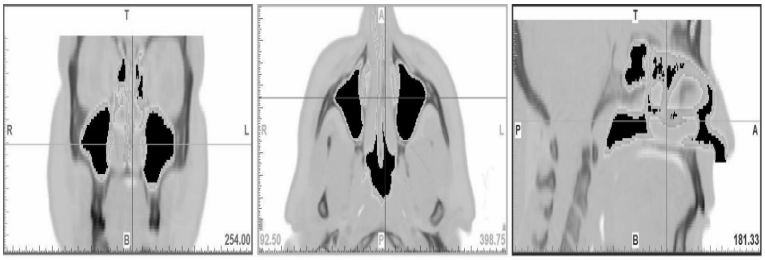

Fig. 1. (a) Coronal, (b) sagittal section of respiratory system.

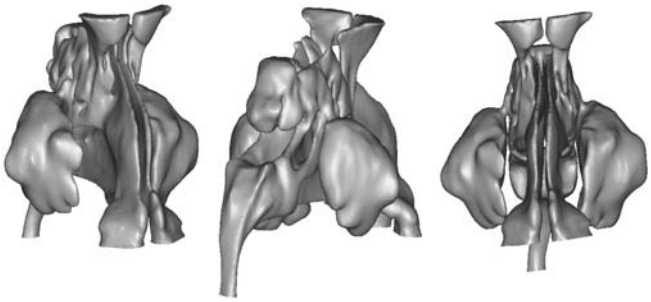

Fig. 2. Different views of 3-D model for the upper respiratory system.

experimentally in vitro and in vivo by many researchers (Zhang *et al.* 2004; Zhang *et al* 2005; Zhang *et al.* 2006; Shi *et al.* 2006; Xi *et al.* 2008; Kleinstreuer *et al.* 2008).

Quantification of the aerosol concentration before and after the upper airways is the essential part of determination of in vivo particle deposition in upper human airways "Cheng (2003). Some researchers are studied particle deposition in the human upper respiration system under a laminar flow regime "Tian *et al.* (2007). It is be noted that for higher respiration rates, the flow field has a turbulent regime leading to turbulent dispersion of particles. In vitro observations using nonrealistic nasal cavities have been used frequently instead of in vivo studies for many years. Recently, airflow and particle transport in human upper respiratory system have been studied in vivo "Proetz (1951) and in vitro "Hahn *et al.* (1993). Because of limitations of in vivo studies due to complex geometry and shape of the nose and upper airways, in vitro methods were used. With the improvement of computational methods in fluid flow simulations and development of computed tomography techniques, many studies on airflows with particle transport in realistic model of nasal cavities have been done and produced valuable data in respiration field "Liu *et al.* (2010). Due to complexity of geometry and unsteady behavior of airflow in nasal cavities, obtained results from computational fluid dynamics are constrained by the geometry. Therefore, these results require validations. For simplicity, most of studies in this area have been focused on only nasal cavity without any sinuses "Koppe *et al.* (2006).

According to the authors' knowledge, a numerical modeling of turbulent flow in three-dimensional realistic model of human upper respiration system have rarely been employed. Thus this research is tried to study of turbulent air flow and particle deposition thru all cavities in human head in details. The realistic model which is used in this research is obtained from CT scan images.

2. GEOMETRY

The model used in this study achieved from CT-scans images of head of a 26-years old woman, from Shahid-Chamran hospital, Shiraz, Iran. It is be noted that according to many researches (Zhao *et al.* 2004; Dahl & Mygind, 1998) the human respiratory systems shape is varying from each person to another, therefore the present model can be changed rapidly to simulate another anatomical deviations. Imaging is helical and performed using a CT-scanner with the following parameters: 99.00 mA, 24.20 cm field of view, 0.625 mm slice increment, and 120 KV. CT image contains wide variety of densities which is denoted various tissues. By tuning the threshold, desired tissue is determined. According to the observations of an expert in each computed tomography scan, the limit between the respiratory tract and the mucus of the upper respiratory tract is determined. Figure 1 shows some examples of sagittal and coronal sections in the upper respiratory tract.

The CT-scan apparatus captured many slices along the direction of human body from inlet of nose to larynx at intervals of 1 to 5 mm. These slices are converted to 3D model that is consist of all components of upper respiratory system. To construct the computational volume, all boundaries are connected and provided faces. Afterward an unstructured mesh consists of tetrahedral cells is generated inside the nasal cavities. The complete 3-D model for the upper respiratory system in the different views are shown in Fig. 2.

3. Governing Equations

3.1 Air Flow Modelling

In order to simulate the turbulent fluid flow in the incompressible and steady-state conditions for the present air way model and typical breathing rates, the low Reynolds number (LRN) k–ω model "Wilcox (1993) is used. Zhang and Kleinstreuer "Zhang and Kleinstreuer (2003) show that it is suitable for internal turbulent flows. Therefore, governing equations are as follows "Zhang and Kleinstreuer (2004):

Continuity equation:

$$\frac{\partial u_i}{\partial x_i} = 0 \tag{1}$$

Momentum equation:

$$\frac{\partial u_i}{\partial t} + u_j \frac{\partial u_i}{\partial x_i} = -\frac{1}{\rho}\frac{\partial p}{\partial x_i} + \frac{\partial}{\partial x_j}\left[(v + v_T)\left(\frac{\partial u_i}{\partial x_j} + \frac{\partial u_j}{\partial x_i}\right)\right] \tag{2}$$

Turbulent kinetic energy equation (k):

$$\frac{\partial k}{\partial t} + u_j \frac{\partial k}{\partial x_j} = \tau_{ij}\frac{\partial u_i}{\partial x_j} - \beta^* k\omega + \frac{\partial}{\partial x_j}\left[(v + \sigma_k v_T)\frac{\partial k}{\partial x_j}\right] \tag{3}$$

Pseudo-vortices equation (ω):

$$\frac{\partial \omega}{\partial t} + u_j \frac{\partial \omega}{\partial x_j} = \alpha\frac{\omega}{k}\tau_{ij}\frac{\partial u_i}{\partial x_j} - \beta\omega^2 + \frac{\partial}{\partial x_j}\left[(v + \sigma_\omega v_T)\frac{\partial \omega}{\partial x_j}\right] \tag{4}$$

It is be noted that summation notation i, j = 1, 2, 3 demonstrate the components of the velocity vector and the spatial coordinates. Turbulent viscosity and its formulation are presented in details in Ref. "Zhang and Kleinstreuer (2004). It is noted that in this study, steady-state condition is applied, therefore first terms in Eqs. (2) through (4) are ignored.

3.2 Model of particle transport

The particle diameter that is used in this study is 5-30 μm. Due to the small size of particles in this range, inertial and gravitational effect are negligible. So, particle transport is affected by the air flow strongly. Lagrangian approach is used to simulate the particle trajectory. The forces that is act on the each particle can be mentioned as follows: drag force $\vec{F}_D$, buoyancy force $\vec{F}_B$, virtual mass force $\vec{F}_{VM}$, and pressure gradient force $\vec{F}_P$.

Because of size and density of particles, all of acting forces except drag and buoyancy forces are negligible. Therefore, the equation of the particle motion is achieved as follows "Xiangdong *et al.* (2012):

$$m_P \frac{d\vec{U}_P}{dt} = \vec{F}_D + \vec{F}_B \tag{5}$$

Drag force:

$$\vec{F}_D = \frac{1}{2} C_D \rho A_P \left|\vec{U} - \vec{U}_P\right| (\vec{U} - \vec{U}_P) \tag{6}$$

Buoyancy force:

$$\vec{F}_B = (m_P - m)\vec{g} = \frac{\pi}{6} d_P^3 (\rho_P - \rho)\vec{g} \tag{7}$$

A_P and C_D are the projected area in the flow direction and the drag coefficient (Schiller and Naumann 1977; King *et al.* 2010) respectively.

4. Numerical Method

4.1 Discretization Schemes

The solutions of the governing equations are carried out with a computational code based on finite-volume method (FVM) that may have the most efficient component to simulate the air movement into the airways. To reach this goal, 3D high accurate model of human head airways was used.

The computational code uses an unstructured multi block mesh. In the present simulation, the PISO (Pressure Implicit Splitting of Operators) algorithm used to solve the governing equations "Issa (1986). Also, many researchers such as Ref. "Chen *et al.* (2009) shows that the Wilcox's k-ω urbulence model is suitable for airflow modeling in respiratory systems. This model provides acceptable accuracy with lower computational cost in these situations. All variables of fluid flow are located at the centers of the control volumes. An improved Rhie–Chow method "Tasri (2010) is used to determine the flow variables on the control volume faces. A 2nd order upwind scheme is employed to model the convective terms of the governing equations. The computational mesh has a high concentration near the model walls in order to capture the thickness of the viscous sublayer zone. As a requirement of LRN turbulence modeling, the first grid point above the wall is given a value of $y^+<1$, where y^+ and u_τ are defined as follows:

$$y^+ = \frac{u_\tau y}{\upsilon} \tag{8}$$

$$u_\tau = \left(\frac{\tau_w}{\rho}\right)^{1/2} \tag{9}$$

Initially, a mesh with 92000 tetrahedral cells is used to compute the velocity domain at an inlet velocity of 1.667 m/s. The topological form of grid is determined by refining the grid until grid independence condition of the solution is achieved. The model is improved by cell adaptation methods using refinement of large volume cells. In this method the cells that have high velocity gradients are refined. This process is repeated twice. Therefore, each repeat producing a model with a higher cell count than the previous one. Afterward, six different gird are produced, 92000, 675000, 1154000, 1600000, 2042000 and 2296113 cells. The grid independence condition according to mean velocity and wall shear stresses satisfies by the model with resolution of 2042000 cells. Therefore,

a model with 2042000 cells is used in this research.

4.2 Boundary Conditions

The creation of physical or computational models requires the identification of the boundaries and setting the appropriate values for them. Air ways in nasal cavities have boundaries those are varies with time and usually covered with a thin layer of mucus. Also external shape of the nose affects the internal flow due to inspiration cycle and flow entering the nares. In breathing cycle, airways below the nasopharynx is impressed. Due to mentioned complexity and according to the authors knowledge there is no model has been attempted to cover all these features yet.

In the present work, three different constant flow entrance velocities of 0.555, 1.111 and 1.667 m/s are used as an inlet condition to simulate the usual breathing occurring during sleeping, resting, and relaxed situations. Also, atmospheric pressure condition is set at the outlet. As mentioned before gravitational acceleration effect is ignored and no-slip condition is used on the model walls.

Initial values for k and ω at the inlet are determined using the following relations "AEA Technology CFX-4.4 (2001):

$$k = 1.5(I \times u_{in})^2 \tag{10}$$

$$\omega = k^{0.5}/0.3D_h \tag{11}$$

Where D_h is the hydraulic diameter and I is the turbulence intensity obtained from following equations "Kang and Greif (1992):

$$I = 0.16\,Re^{-1/8} \tag{12}$$

4.3 Model Validation

Comparisons between computational and experimental velocity profiles is necessary for accurate simulation. Some experimental measurements are available for resting conditions of Q_{in} =10 L/min "Johnstone *et al.* (2004). Also, for this case, numerical simulation with two turbulence model is done by Zhang and Kleinstreuer "Zhang and kleinstreuer (2011). In their model, because of complexity, some details of geometry are ignored and model is simplified. Figure 3 shows comparisons of measured average and computational velocity profiles in the airway model with Q_{in}=10 L/min or approximately u_{in}=1.111 m/s. In this figure y' is defined as y / √A where A is the area of cross section.

As presented, the average velocity profiles obtained with the shear stress transport and large eddy simulation model are in reasonable agreement with the measured data. But the results of the present work with k-ω model have the better accuracy respect to the other data. The reason of this better agreement is the more complexity and more details of geometry and its refine meshes. But any disagreement between simulations results and measurements data may be due to imperfect repetitions of the measurement locations in simulations, and the stationary hot wire probes used in the experiments being incapable of discriminating the considerable reverse flow in this region "Doorly *et al.* (2008). Also, physiological observations in medical sciences shows that the particles in micro and Nano scales can be escaped from the upper respiratory system and about ten percent of these particles are blocked by nose "Hall (2011). Particle efficiency validates these observations. Therefore, obtained results are reliable.

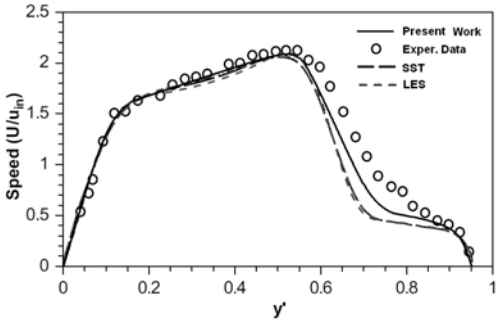

Fig. 3. Comparison between simulated axial velocity profiles at plane 4 in nasal cavity model at u_{in}=1.111 m/s and experimental measurements "Johnstone *et al.* (2004) and previous numerical results "Zhang and Kleinstreuer (2011).

5. Results And Discussions

Three different air velocities (0.555, 1.111, and 1.667 m/s), are investigated in this study. These velocities are choose to cover a wide range of the normal respiration during resting conditions. The flow regime has laminar regime for air velocity of 0.555 m/s and turbulent for other velocities. Figure 4 shows the planes location which is used in the presentation of results.

5.1 Airflow

Figure 5 demonstrates the simulated airflow streamlines in human nasal cavities for a respiration speed of 1.111 m/s. Air enters into the vestibule region from the nostril and then turns approximately about a 90 degree and shows that multiple secondary flows that formed in the lower region from the main flow locally that flow in the middle region. Also, the main part of the flow hold near the septum walls in this region and only a little amount of it reached the olfactory.

Streamlines show that the air tend to flow thru upper part of airways due to effect of centrifugal forces. But this part of airways is very small, so as shows in Fig. 6, main of the air, flows in the middle of this region. As depicted in Figs. 7 and 8, after the air flow reaches to the nasal valve region, the air develops and mostly flows thru the middle meatus area. A small amount of air flows thru the olfactory and superior meatus. Refer to "Johnstone *et al.* (2004) to find more details about air flow in human upper airways. After the air flows thru the nasopharynx turns approximately about 90 degree again in the vertical direction. In this situation

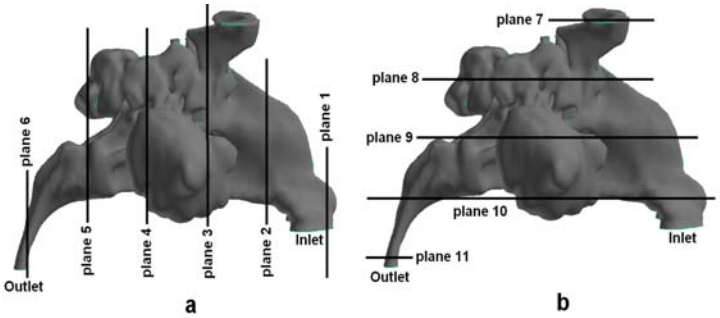

Fig. 4. Planes for presentation of results.

centrifugal forces increase the amount of air in the upper part of pharynx and then flow becomes developed approximately. The minimum value of cross section area occurs at the end of nasopharynx. Therefore, velocity has a maximum value in this region. Figures 9 through 11 show the velocity contours for planes 8, 9 and 11 respectively. As depicted in Fig. 10, within the first 2–3 cm of the air passage, nasal cavity resistance is almost up to half of the total airways resistance. For example, in Fig. 10a the inlet velocity is 0.555 m/s and the mean velocity of a plane 9 (approximately 2-3 cm above the nose inlet) this velocity is reduced to 0.23 m/s. same results is observed in the Figs. 10b and 10c.

Fig. 5. Airflow streamlines for breathing speed of 1.111 m/s.

5.2 Micro-Particle Deposition

In this study, micro particle deposition in the nasal cavity is calculated. For calculation of particle deposition, we used a constant inhalation average flow rate. Total deposition is calculated for four different particle sizes of 5, 10, 15 and 30 μm. The simulation result is displayed in Fig. 12. This figure shows the path of each particle through the nasal cavity. Along the axial direction of the airway, results show a general trend for the cross-sectional area profiles. Some particles are blocked to move due to geometry and its momentum and where geometry of human upper airways begins to enlarge, many of the vortices are formed in the upper olfactory and only posterior to the nasal valve as showed in Fig. 12.

Particle efficiency is defined as the ratio between blocked or deposited particles to all particles. For six different cases which is considered in this study, particle efficiency is computed and presented in Table 1.

Table 1 Particle deposition efficiency

Particle diameter (μm)	5	10	15	30
Airflow velocity (m/s): 0.555	% 4.9	% 5.6	% 6.1	% 6.3
Airflow velocity (m/s): 1.111	% 4.1	% 4.6	% 5.1	% 5.2
Airflow velocity (m/s): 1.667	% 3.7	% 4.3	% 4.8	% 5.1

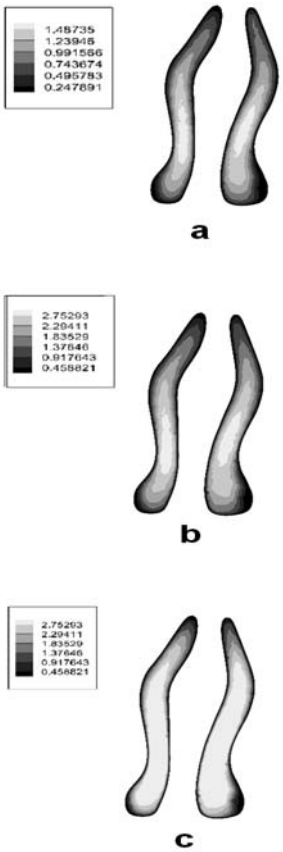

Fig. 6. Velocity contours on plane 2 (a) u_{in}=0.555 $m.s^{-1}$, (b) u_{inlet} = 1.111 $m.s^{-1}$, (c) u_{inlet} = 1.667 $m.s^{-1}$.

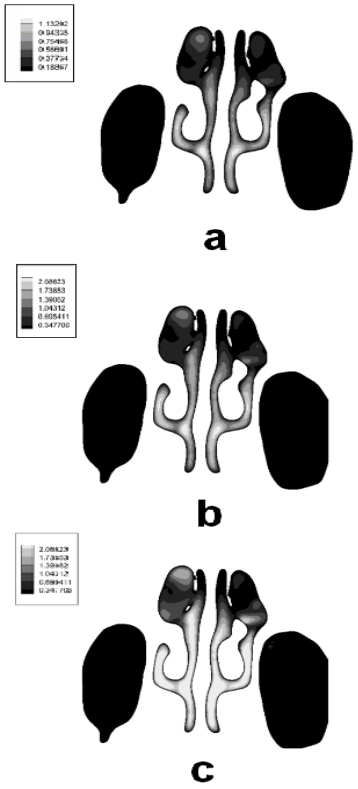

Fig. 7. Velocity contours on plane 4 (a) u_{in}=0.555 m.s^{-1}, (b) u_{inlet} = 1.111 m.s^{-1}, (c) u_{inlet} = 1.667 m.s^{-1}.

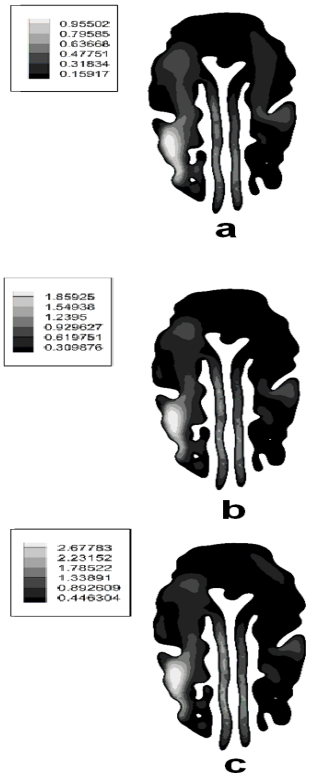

Fig. 9. Velocity contours on plane 8 (a) u_{in}=0.555 m.s^{-1}, (b) u_{inlet} = 1.111 m.s^{-1}, (c) u_{inlet} = 1.667 m.s^{-1}.

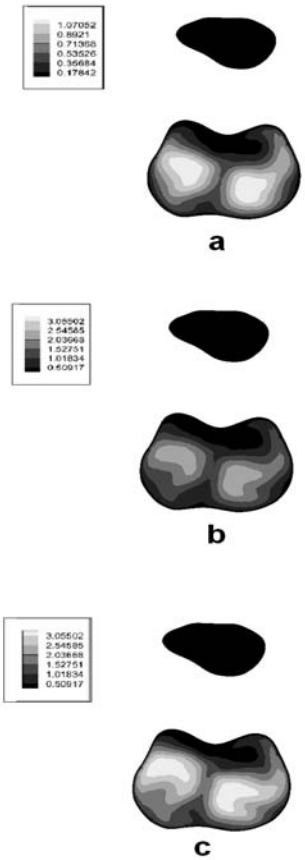

Fig. 8. Velocity contours on plane 5 (a) u_{in}=0.555 m.s^{-1}, (b) u_{inlet} = 1.111 m.s^{-1}, (c) u_{inlet} = 1.667 m.s^{-1}.

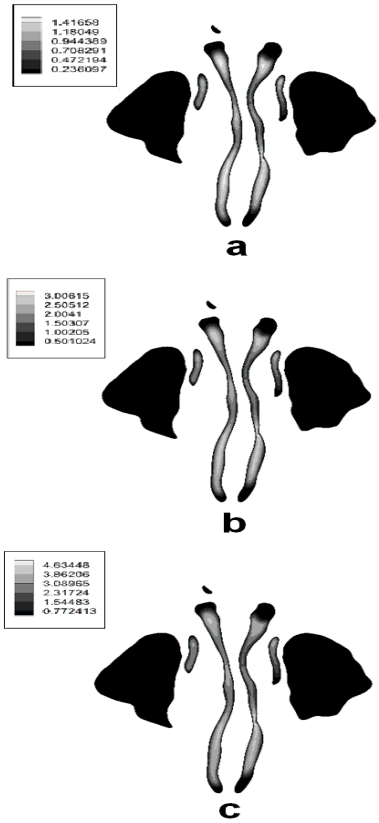

Fig. 10. Velocity contours on plane 9 (a) u_{in}=0.555 m.s^{-1}, (b) u_{inlet} = 1.111 m.s^{-1}, (c) u_{inlet} = 1.667 m.s^{-1}.

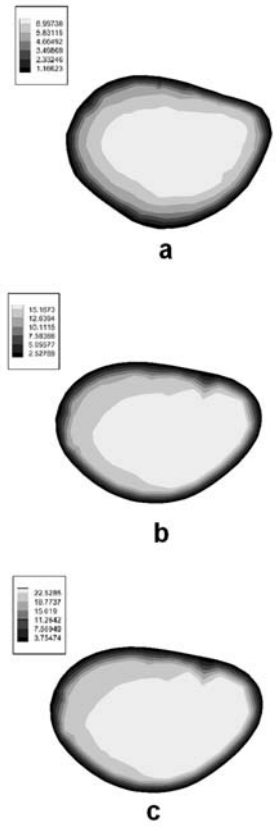

Fig. 11. Velocity contours on plane 11 (a) u_{in}=0.555 m.s^{-1}, (b) u_{inlet} = 1.111 m.s^{-1}, (c) u_{inlet} = 1.667 m.s^{-1}.

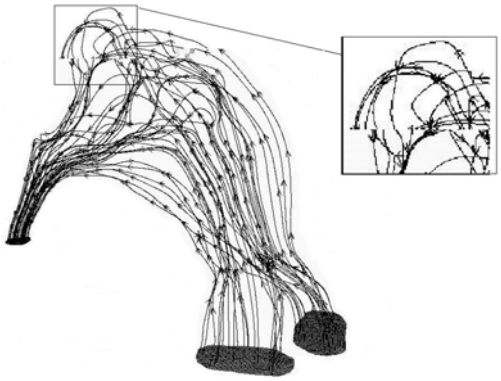

Fig. 12. Particle deposition for 15 µm diameter and u_{in}=0.555 m.s^{-1}.

6. CONCLUSION

To learn more about the structure of the upper respiratory system, the air flow and particle deposition is investigated and compared with available experimental and numerical data. The simulation based on the computed tomography scans of a 26th age woman.

- Along the axial direction of the airway, results show a general trend for the cross-sectional area profiles.
- Within first 2–3 cm of the air passage, nasal cavity resistance is almost more than fifty percent of the total airways resistance.
- Where geometry of human upper airways begins to enlarge, many of the vortices are formed in the upper olfactory and only posterior to the nasal valve.
- Results show that multiple secondary flows that formed in the lower region from the main flow locally that flow in the middle region.
- The main part of the flow hold near the septum walls in this region and only a little amount of it reached the olfactory.
- Results show that particle deposition efficiency is increased when particle diameter is increased, but physiological observations in medical sciences shows that the particles in micro and Nano scales can be escaped from the upper respiratory system as presented in Table 1.

ACKNOWLEDGEMENTS

The authors would like to convey their gratefulness to the staff of Shahid-Chamran Hospital and Taaba Tomography Center, Shiraz, Iran regarding to their help to achieving CT Scans data.

REFERENCES

AEA Technology CFX-4.4: Solver. *Oxford shire*, UK, Canonsburg, PA, 2001.

Chen, X. B., H. P. Lee, V. F. H. Chong and D. Y. Wang (2009). Assessment of septal deviation effects on nasal air flow: a computational fluid dynamics model. *Laryngoscope* (119), 1730–1736.

Cheng, Y. S. (2003). Aerosol deposition in the extra thoracic region. *Aerosol Sci Tech* (37), 659–671.

Dahl, R., and N. Mygind (1998). Anatomy, physiology and function of the nasal cavities in health and disease, *Adv. Drug Deliv. Rev.* (29), 3-12.

Doorly, D. J., D. J. Taylor and R. C. Schroter (2008). Mechanics of airflow in the human nasal airways, *Respir. Physiol. Neurobiol.* (163), 100–110.

Hahn, I., P. W. Scherer and M. M. Mozell (1993). Velocity profiles measured for airflow through a large-scale model of the human nasal cavity. *J App Physiology* (75), 2273-2287.

Hall, J. E. (2011) Guyton and Hall Textbook of Medical Physiology, 12th ed., *Elsevier*, New York.

Issa, R. I. (1986). Solution of the implicitly discretised fluid flow equations by operator splitting, *J. Comput. Phys.* (62) 40–65.

Johnstone, A., M. Uddin, A. Pollard and A. Heenan (2004). Finlay WH The flow inside an idealised form of the human extra-thoracic airway, *Exp in Fluids* (37), 673–689.

Kang, S. H. and R. Greif (1992). Flow and heat transfer to a circular cylinder with a hot impinging air jet, *Int J Heat Mass Transf* (35), 2173-2183.

King, C. M., K. Inthavong and J. Tu (2010). Inhalability of micron particles through the nose and mouth. *Inhalation Toxicology* (22), 287-300.

Kleinstreuer C., Z. Zhang, and J.F. Donohue (2008). Targeted drug-aerosol delivery in the human respiratory system. *Annu. Rev. Biomed. Eng.* (10), 195-220.

Koppe, T., C. Weigel, M. Baerenklau, W. Kaduk, T. Bayerlein and T. Gedrange (2006). Maxillary sinus pneumatization of an adult skull with an untreated bilateral cleft palate. *J Cranio-Maxillofacial Surgery* (34), 91-95.

Liu, Y., E. A. Matida and M. R. Johnson (2010). Experimental measurements and computational modeling of aerosol deposition in the Carleton-Civic standardized human nasal cavity. *J Aerosol Sci* (41), 569-586.

Proetz, A. W. (1951). Air currents in the upper respiratory tract and their clinical importance. *Annals Otology Rhinology Laryngology* (60), 439-467.

Schiller, L. and Z. Naumann (1977). A drag coefficient correlation. *Zeitschrift Des Vereines Deutscher Ingenieure*.

Shi, H., C. Kleinstreuer and Z. Zhang (2006). Laminar airflow and nanoparticle or vapor deposition in a human nasal cavity model. *J Biomech. Eng.-Trans ASME* (128), 697-706.

Tasri, A. (2010). Simple improvement of momentum interpolation equation for Navier-Stoke equation solver on unstructured grid. *J Math Statistics* (6), 265-270.

Tian, Z. F., K. Inthavong and J. Y. Tu (2007). Deposition of inhaled wood dust in the nasal cavity. *InhalToxicol* (19), 1155–65.

Wilcox, D. C. (1993). Turbulence Modeling for CFD. *DCW Industries Inc*, LA Canada, CA.

Xi, J. X. and P. W. Longest (2008). Evaluation of a drift flux model for simulating sub-micrometer aerosol dynamics in human upper tracheobronchial airways. *Annals Biomedical Eng.* (36), 1714–1734.

Xiangdong, L., I. Kiao and T. Jiyuan (2012). Particle inhalation and deposition in a human nasal cavity from the external surrounding environment. *Building and Environment* (47), 32-39.

Zhang, Z. and C. Kleinstreuer (2003). Low Reynolds number turbulent flows in locally constricted conduits: a comparison study, *AIAA J.* (41), 831–840.

Zhang, Z. and C. Kleinstreuer (2004). Airflow structures and nano-particle deposition in a human upper airway model. *J Comp Physics* (198), 178–210.

Zhang, Z., C. Kleinstreuer, J.F. Donohue, and C.S. Kim (2005). Comparison of micro- and nano-size particle depositions in a human upper airway model. *J Aerosol Sci* (36), 211-233.

Zhang, Z., C. Kleinstreuer, and C.S. Kim (2006). Water vapor transport and its effect on the deposition of hygroscopic droplets in a human upper airway model. *Aerosol Sci Tech* (40), 1-16.

Zhang, Z. and C. Kleinstreuer (2011). Computational analysis of airflow and nanoparticle deposition in a combined nasal–oral–tracheobronchial airway model, *J Aerosol Sci* (42), 174-194.